RSC Advances

PAPER

View Article Online
View Journal | View Issue

Cite this: *RSC Adv.*, 2018, **8**, 3264

Simultaneous removal of Sb(III) and Cd(II) in water by adsorption onto a $MnFe_2O_4$–biochar nanocomposite†

Yu-Ying Wang,[ab] Hai-Yang Ji,[ac] Hao-Hao Lu,[ab] Yu-Xue Liu,[ab] Rui-Qin Yang,[de] Li-Li He[ab] and Sheng-Mao Yang *[abc]

Received 8th December 2017
Accepted 2nd January 2018

DOI: 10.1039/c7ra13151h

rsc.li/rsc-advances

In this study, a jacobsite–biochar nanocomposite ($MnFe_2O_4$–BC) was fabricated and used to simultaneously remove Sb(III) and Cd(II) from water *via* adsorption. The $MnFe_2O_4$–BC nanocomposite was prepared *via* a co-precipitation method and analyzed using various techniques. The results confirm the successful decoration of the biochar surface with $MnFe_2O_4$ nanoparticles. The maximum Sb(III) removal efficiency was found to be higher from bi-solute solutions containing Cd(II) than from single-solute systems, suggesting that the presence of Cd(II) enhances the removal of Sb(III). The Langmuir isotherm model describes well Sb(III) and Cd(II) removal *via* adsorption onto the $MnFe_2O_4$–BC nanocomposite. The maximum adsorption capacities are 237.53 and 181.49 mg g^{-1} for Sb(III) and Cd(II), respectively, in a bi-solute system. Thus, the prepared $MnFe_2O_4$–BC nanocomposite is demonstrated to be a potential adsorbent for simultaneously removing Sb(III) and Cd(II) ions from aqueous solutions.

1. Introduction

The introduction of antimony (Sb) and cadmium (Cd) into the environment, mainly from anthropogenic activities like mining and industrial work, has created global concern.[1,2] Sb, a hazardous substance, may lead to pneumoconiosis and have carcinogenic effects on human health.[1,3] The maximum permissible Sb concentrations in drinking water are 5, 6 and 10 μg L^{-1}, as established by China, the United States Environmental Protection Agency and the European Union, respectively.[4] Moreover, there are two inorganic species (Sb(III) and Sb(V)) of Sb in aquatic systems. Of these, Sb(III) is more toxic than Sb(V) by a factor of ten.[5] Cd is one of the most toxic heavy metals, and has received significant attention in recent years.[6] Cd is ubiquitous, and over-exposure to Cd can cause bone and kidney damage.[7] According to guidelines from the World Health Organization, the maximum contaminant level (MCL) of Cd(II) in drinking water should be limited to 3 μg L^{-1}.[2] Alarmingly, Sb and Cd generally coexist in many sources, such as tailing heaps, water, and sediments.[5,8] For instance, combined Sb and Cd pollution is frequently observed in Xikuangshan, because of the concomitant presence of Cd in Sb-containing ores.[8] Moreover, Sb and Cd are the most abundant heavy metal contaminants threatening some cities in the Guangxi province of China.[9] The coexistence of Sb and Cd might pose a higher risk to human health and ecological safety than their individual presence. In addition, the processes required for the simultaneous removal of Sb and Cd might also differ from those used for removal from systems containing only Sb or Cd. Despite this, investigations into the simultaneous removal of Sb(III) and Cd(II) are rare.

It is widely known that adsorption technologies are promising for the elimination of contaminants from aqueous solutions. Biochar is an inexpensive carbon-rich material that might widely be used in adsorbent systems, and is produced through the pyrolysis of biomass under oxygen-free or oxygen-limited conditions.[10,11] Biochar has a large specific surface area and porous structure, as well as abundant surface functional groups and mineral components; thus, it is a potential adsorbent for pollutants. Because most biochar presents a predominantly net negatively charged surface,[12,13] its ability to remove aqueous Sb, which is in anionic form, may be relatively weak. Therefore, several methods have been developed to modify biochar to enhance its anion adsorption capabilities. Biochar modified with iron oxide or manganese oxide has been reported to show strong ability in removing Sb from aqueous solutions.[4] For instance, Xu *et al.* investigated the capabilities for and

[a]*Institute of Environment, Resource, Soil, and Fertilizer, Zhejiang Academy of Agricultural Sciences, Hangzhou, 310021, P. R. China. E-mail: yangshengmao@263.net; Fax: +86 571 86419218; Tel: +86 571 86419218*

[b]*Engineering Research Center of Biochar of Zhejiang Province, Hangzhou, 310021, P. R. China*

[c]*College of Chemistry and Life Sciences, Zhejiang Normal University, Jinhua, 321004, P. R. China*

[d]*Zhejiang Provincial Collaborative Innovation Center of Agricultural Biological Resources Biochemical Manufacturing, Zhejiang University of Science and Technology, Hangzhou, 310023, P. R. China*

[e]*Zhejiang Provincial Key Lab for Chem & Bio Processing Technology of Farm Product, Zhejiang University of Science and Technology, Hangzhou, 310023, P. R. China*

† Electronic supplementary information (ESI) available. See DOI: 10.1039/c7ra13151h

mechanisms involved in the removal of Sb(III) using Fe–Mn binary oxides, ferric hydroxide, and manganese dioxide.[4] Bai *et al.* investigated potential oxidation and adsorption pathways for Sb(III and V) species in the presence of Mn(II) and Mn-oxidizing bacteria, with or without Fe(II), and found that *in situ* formed biogenic Mn oxide and Fe–Mn oxides could effectively remove Sb.[14] Qi and Pichler studied the sequential and simultaneous adsorption of Sb(III) and Sb(V) on ferrihydrite, and demonstrated that ferrihydrite is an effective adsorbent for Sb(III) and Sb(V) in single and binary systems, with a higher efficiency toward Sb(III) than Sb(V).[15] However, despite the evident potential interference of Sb(III) into the adsorption of Cd(II) and the coexistence of Sb(III) and Cd(II) in water samples, the adsorption behavior of this important binary system on Fe and Mn modified biochar has not been reported to date.

In this study, a jacobsite–biochar nanocomposite ($MnFe_2O_4$–BC) was synthesized and used to evaluate the co-adsorption performance of Sb(III) and Cd(II). The effects of various experimental conditions, such as solution pH, contact time, initial concentration, and coexisting ions, on their adsorption were investigated. A possible mechanism for Sb(III) and Cd(II) adsorption on the $MnFe_2O_4$–BC nanocomposite is also proposed. Thus, our results may contribute to the development of decontamination technologies targeting Sb(III)/Cd(II) polluted water, while deepening our understanding of the adsorption of Sb(III) and Cd(II) on biochar materials.

2. Materials and methods

2.1 Materials

All chemical regents used in this study were of analytical reagent (AR) grade. Stock solutions of 1000 mg L^{-1} Sb(III) ($KSbC_4H_4O_7$) and Cd(II) ($Cd(NO_3)_2 \cdot 4H_2O$) were prepared with deionized water. The required concentrations for working solutions were obtained through diluting the Sb(III) and Cd(II) stock solutions.

2.2 Preparation of $MnFe_2O_4$–BC

The biochar used in this study was obtained from tea branches through a typical slow pyrolysis process.[16] Briefly, a tea branch was loaded into a programmable tube furnace and pyrolyzed under anaerobic conditions at 500 °C at a heating rate of 25 °C min^{-1} for 90 min. After carbonization, the biochar was cooled naturally to room temperature to obtain the pristine BC samples used in the experiments. The $MnFe_2O_4$–BC nanocomposite was prepared *via* a co-precipitation method. Briefly, 8.34 g (0.3 M) of $FeSO_4 \cdot 7H_2O$ was dissolved in 100 mL of deionized water, and 1 g of the prepared BC was added to obtain suspension A. Then, 1.58 g (0.1 M) of $KMnO_4$ was dissolved in 100 mL of deionized water under vigorous stirring to obtain solution B. Finally, solution B was added to suspension A under continuous stirring. During the reaction, an appropriate amount of NaOH solution was added to maintain the pH of the solution at about 10. The resulting slurry was aged at room temperature for 3 h, then centrifuged and washed with deionized water to remove excess salt. After that, the product was vacuum dried overnight at 25 °C.

2.3 Characterization

pH Values were measured using a pH meter (Mettler Toledo FE28), supplied with a combined electrode. Field emission electron microscopy (FESEM) images of BC and $MnFe_2O_4$–BC were gained using a field emission electron microscope (Hitachi S-4800). Fourier transform infrared spectra (FT-IR) were recorded using a Nicolet 380 spectrometer. An X-ray diffractometer (Bruker D8 Advance) was used to collect X-ray diffraction (XRD) patterns of the samples. The specific surface area was measured using a Nova 2000e surface area analyzer (Quantachrome, USA). A Thermo Scientific K-Alpha spectrometer was used to obtain X-ray photoelectron spectra (XPS) of $MnFe_2O_4$–BC after adsorption.

2.4 Adsorption experiments

All adsorption experiments were carried out in triplicate at 298 K, and averaged values of the results are reported. The influence of the pH of the initial solution, adsorption kinetics, adsorption isotherms, ionic strength, and competing ions on Sb(III) and Cd(II) adsorption were analyzed. The influence of pH on the adsorption abilities of BC and $MnFe_2O_4$–BC was examined over the pH range of 3–7. Acidic pH was mainly selected because $Cd(OH)_2$ has relatively low solubility in basic media. HCl and/or KOH were used to adjust the pH of solutions.

Kinetic experiments were carried out at room temperature. Mixed solutions consisting of 50 mL of Sb(III) and Cd(II) (50 mg L^{-1}) were added to a 100 mL conical flask, and the pH of the resulting solution was adjusted to an optimum pH value using 0.1 mol L^{-1} HCl and/or KOH. Then, 50 mg of BC or $MnFe_2O_4$–BC was added to the solutions. The conical flasks were shaken using a thermostatically controlled shaker (ZWYR-2102C) at 120 rpm for different time intervals (10, 30, 60, 180, 300, 540, 720, and 1440 min).

Sb(III) and Cd(II) adsorption isotherms were obtained for Sb(III) and Cd(II) mixed solutions (50 mL) in 100 mL conical flasks *via* batch tests. The initial concentration of the mixture was varied from 25 to 500 mg L^{-1}. 50 mg of BC or $MnFe_2O_4$–BC was added to the conical flask after the pH of the solution was adjusted to an optimum pH value. The pH of the solution was adjusted by adding 0.1 mol L^{-1} HCl and/or KOH. Then, the conical flasks were shaken using a thermostatically controlled shaker at 120 rpm at room temperature for 24 h.

The influence of ionic strength on the removal of Sb(III) and Cd(II) was also investigated by adjusting the ionic strength of solution to 0, 0.001, 0.005, 0.01, 0.05, 0.1 and 0.5 M, using KCl.

The effects of five common coexisting cations, K^+, Ca^{2+}, Mg^{2+}, PO_4^{3-}, and NO_3^-, were also investigated by adding 0.01 M KCl, $CaCl_2$, $MgCl_2 \cdot 6H_2O$, $NH_4H_2PO_4$, and KNO_3 to mixed solutions containing 50 mg L^{-1} Sb(III) and Cd(II) in separate conical flasks. After the adsorption experiments, all samples were filtered, and then the filtrates were analyzed using inductively coupled plasma-atomic emission spectroscopy (ICP-AES, Prodigy). The removal efficiencies (U, %) and equilibrium adsorption amounts of Sb(III) and Cd(II) (q_e, mg g^{-1}) were calculated using the following equations:

$$U\% = \frac{(C_0 - C_e)100\%}{C_0} \quad (1)$$

$$q_e = \frac{(C_0 - C_e)V}{W} \quad (2)$$

where C_0 is the initial concentration of Sb(III) or Cd(II) (mg L^{-1}), C_e is the equilibrium concentration of Sb(III) or Cd(II) (mg L^{-1}), W is the weight of the biochar (mg), and V is the volume of the solution (mL).

2.5 Adsorbent reuse

To test the reusability of $MnFe_2O_4$–BC, five consecutive cycles were performed in triplicate. Each adsorption process was carried out as batch experiments for 24 h, and then $MnFe_2O_4$–BC was separated using centrifugation. Prior to the next cycle, the collected adsorbent was washed repeatedly to remove residual solution.

3. Results and discussion

3.1 Characterization of the $MnFe_2O_4$–BC nanocomposite

Fig. 1a depicts XRD patterns of BC and $MnFe_2O_4$–BC. The broad peak located at about 24° in the XRD pattern of BC represents a typical amorphous carbon diffraction pattern.[17] In addition, the XRD pattern of BC has a peak at 29.5°, which is attributed to $CaMg(CO_3)_2$/dolomite.[18] For $MnFe_2O_4$–BC, new diffraction peaks are observed at 29.76°, 35.05°, 42.59°, 56.26°, and 61.68°, corresponding to d values of 3.00 Å, 2.56 Å, 2.13 Å, 1.64 Å and 1.50 Å, respectively, which are indexed to $MnFe_2O_4$, with JCPDS card no. 742403. This result suggests that $MnFe_2O_4$ nanoparticles have been loaded on the surface of the biochar. The corresponding FT-IR spectra of BC and $MnFe_2O_4$–BC are exhibited in Fig. 1b. The band in the range of 3000–3445 cm^{-1} may be due to the stretching vibrations of the O–H groups of water.[19,20] The peaks at about 1424 cm^{-1} for BC and at 1454 cm^{-1} for $MnFe_2O_4$–BC in the FT-IR spectra were assigned to $-CH_2-$ groups, while the peak at about 1604 cm^{-1} represents the aromatic C=C and C=O stretching vibrations.[21] These organic functional groups may be attributed to the lignin structure of tea branches. Compared to the FT-IR spectrum of BC, new peaks at approximately 578 cm^{-1} and 420 cm^{-1} appear in the FT-IR spectrum of $MnFe_2O_4$–BC. These two peaks can be identified as the infrared absorption peaks of $MnFe_2O_4$.[22] Bujoreanu *et al.* showed that the IR peaks between 600 and 400 cm^{-1} for $MnFe_2O_4$ mainly depend on the vibrations of the octahedral group.[23] Therefore, the results from the FT-IR spectrum are consistent with the XRD results presented in Fig. 1a, and further confirm the successful loading of $MnFe_2O_4$ nanoparticles on BC.

The morphologies of BC and $MnFe_2O_4$–BC were characterized using FESEM, and representative images are shown in Fig. 1c and d. As shown in Fig. 1c, BC derived from tea branches is composed of irregular sheets, with some small granules attached to the sheet surface. The corresponding energy-dispersive X-ray (EDX) spectroscopic analysis (inset of Fig. 1c) suggests that the BC sample contains carbon, oxygen, and a small quantity of potassium. Moreover, FESEM/EDX analyses of $MnFe_2O_4$–BC suggest that $MnFe_2O_4$ particles are present on the biochar surface (Fig. 1d). The SEM image clearly shows that many small aggregates/particles are present on the surface of $MnFe_2O_4$–BC (Fig. 1d). The EDX analysis of $MnFe_2O_4$–BC indicates that these nanoparticles contain carbon, oxygen, iron, and manganese, as well as small amounts of sodium, chlorine, potassium, and calcium (Fig. 1d, inset). Carbon, sodium, chlorine, potassium, and calcium originate from biochar, whereas oxygen, iron, and manganese originate from $MnFe_2O_4$. Thus, the results of XRD, FT-IR, and FESEM characterization clearly demonstrate that $MnFe_2O_4$ particles are successfully loaded onto the surface of the pristine biochar.

N_2 adsorption–desorption isotherms from BC and $MnFe_2O_4$–BC are shown in Fig. 1e. The isotherms are characteristic type IV isotherms with a H3 hysteresis loop. The Brunauer–Emmett–Teller (BET) surface areas of BC and $MnFe_2O_4$–BC were found to be 2.35 and 30.38 $m^2\ g^{-1}$, respectively. The significant increase in BET surface area after modification is expected to enhance the heavy metal adsorption process. In addition, the pore size distributions and total volumes of BC and $MnFe_2O_4$–BC are also determined. The pore size distributions of BC and $MnFe_2O_4$–BC are shown in Fig. 1f. The peak is centered at 30.4 nm for BC, and 3.4 nm for $MnFe_2O_4$–BC. The pore diameter and total pore volume of BC are approximately 19.80 nm and 0.00675 $cm^3\ g^{-1}$, respectively, whereas they are 4.15 nm and 0.033 $cm^3\ g^{-1}$ for $MnFe_2O_4$–BC. These results demonstrate that the prepared BC and $MnFe_2O_4$–BC nanocomposite are mesoporous materials.

3.2 Effects of solution pH

The surface charge of BC and $MnFe_2O_4$–BC, the degree of ionization, and the species ions, Sb(III) and Cd(II), can be affected by the pH of solution. Therefore, the effects of solution pH on the adsorption of Sb(III) and Cd(II) ions onto BC and $MnFe_2O_4$–BC were examined. Considering metal hydrolysis and precipitation, the experiments were carried out at pH values between 3 and 7. Obviously, the adsorption of Sb(III) and Cd(II) by BC was found to be sensitive to variations in solution pH, which generally improved with an increase in pH from 3.0 to 7.0 (Fig. 2a). This could be because biochar contains surface functional groups such as –COOH and –OH (Fig. 1b). The dissociation of these organic functional groups increases upon increasing the pH of the solution, and these functional groups may interact with Sb(III) and Cd(II) to form surface complexes. However, the influence of pH on the removal of Sb(III) by $MnFe_2O_4$–BC was minimal, whereas the adsorption of Cd(II) by $MnFe_2O_4$–BC increased with pH. This suggests that the mechanism of Sb(III) adsorption onto $MnFe_2O_4$–BC is different from that using BC. Based on the uptake by BC and $MnFe_2O_4$–BC, pH 7.0 was chosen as the optimal pH value for Sb(III) and Cd(II) adsorption in subsequent experiments.

3.3 Adsorption kinetics of a bi-solute (Sb + Cd)

To study the kinetics of adsorption of Sb(III) and Cd(II) on BC and $MnFe_2O_4$–BC, the adsorption processes were investigated with respect to contact time. The experimental data were fitted

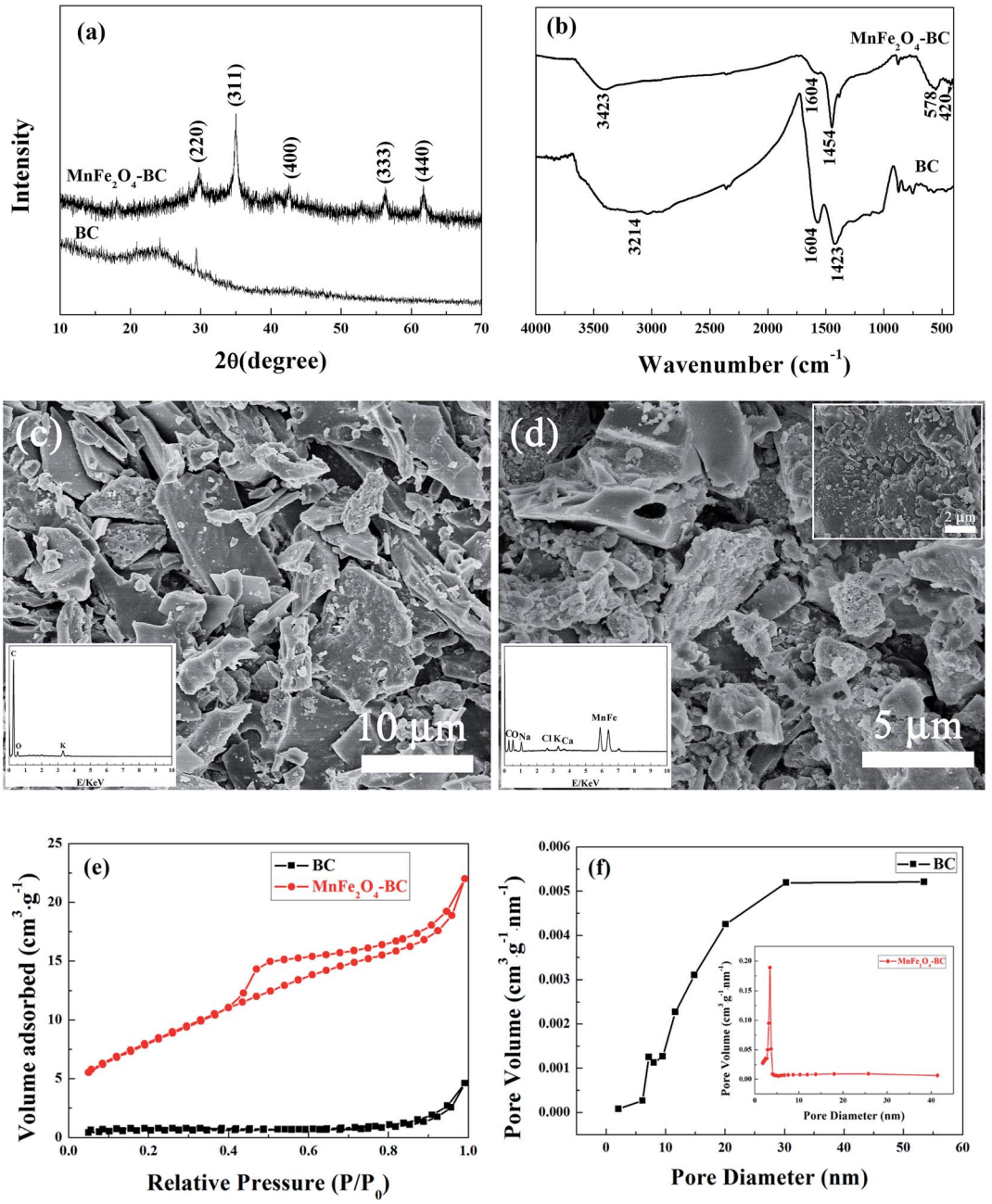

Fig. 1 (a) XRD patterns and (b) FT-IR spectra of BC and $MnFe_2O_4$–BC; (c) FESEM image of BC (inset: EDX spectrum of BC); (d) FESEM image of $MnFe_2O_4$–BC (inset: EDX spectrum of $MnFe_2O_4$–BC); (e) nitrogen adsorption–desorption isotherms of BC and $MnFe_2O_4$–BC; and (f) pore size distributions of BC and $MnFe_2O_4$–BC.

using pseudo-first-order and pseudo-second-order kinetic models,[24] which can be expressed as follows:

$$\log(q_e - q_t) = \log q_e - \frac{tk_1}{2.303} \quad (3)$$

$$\frac{t}{q_t} = \frac{1}{k_2 q_e^2} + \frac{t}{q_e} \quad (4)$$

where q_e and q_t (mg g^{-1}) represent the amount of target ions adsorbed at equilibrium and at time t, respectively. k_1 (min^{-1}) and k_2 (g mg^{-1} min^{-1}) are the adsorption rate constants of the pseudo-first-order and pseudo-second-order kinetic models, respectively.

The kinetic curves are shown in Fig. 2c and d. For BC, the adsorption of Sb(III) is rapid in the first 3 h, and then becomes slower and reaches equilibrium after 12 h (Fig. 2c). In contrast, the adsorption of Cd(II) is slow and reaches equilibrium after 12 h (Fig. 2c). Moreover, the removal of Sb(III) and Cd(II) through adsorption onto pristine BC is poor. Fig. 2d shows that the removal of both Sb(III) and Cd(II) using $MnFe_2O_4$–BC is rapid in the first 1 h and then becomes slow. Adsorption equilibrium is

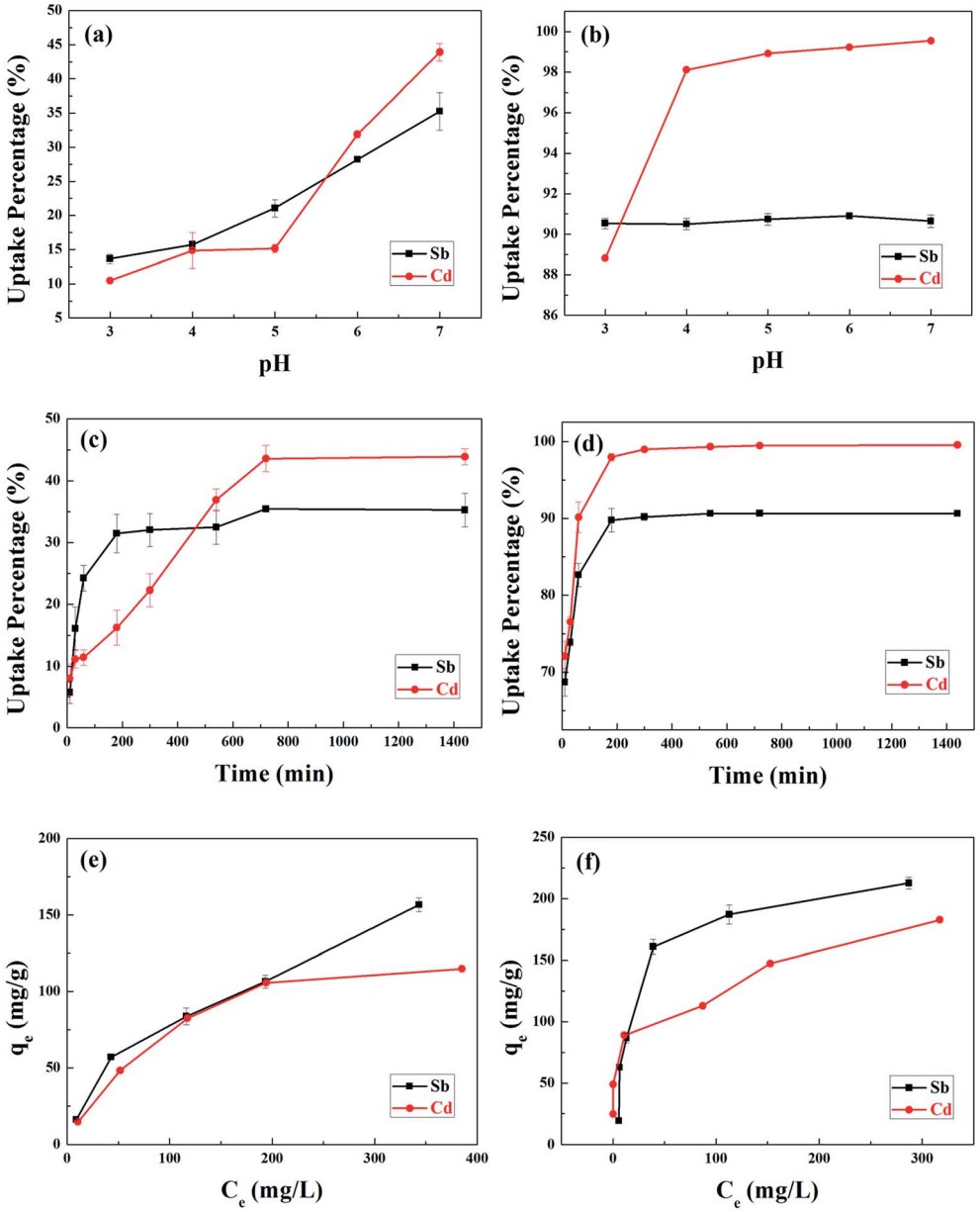

Fig. 2 The effects of pH on the removal of Sb(III) and Cd(II) from a binary system using (a) BC and (b) $MnFe_2O_4$–BC at room temperature for 24 h; the removal of Sb(III) and Cd(II) from a binary system at pH 7.0 using (c) BC and (d) $MnFe_2O_4$–BC at room temperature, after different contact times; and the effects of initial concentration on the removal of Sb(III) and Cd(II) from a binary system at pH 7.0 using (e) BC and (f) $MnFe_2O_4$–BC.

gradually achieved within 5 h for both Sb(III) and Cd(II). This is because there are abundant available sites on the biochar surface during the initial rapid adsorption stage. As adsorption proceeds, Sb(III) and Cd(II) accumulate on the surface of the biochar, resulting in a decrease in the adsorption rate. Moreover, the removal of Sb(III) and Cd(II) using $MnFe_2O_4$–BC is nearly complete, and is much higher than that facilitated by pristine BC. The pseudo-first-order and pseudo-second-order kinetic models were used to fit the experimental data (Fig. 3). The corresponding parameters and correlation coefficients are listed in Table 1. It is clear that the correlation coefficient (R^2) of the pseudo-second-order model is closer to 1 and is higher than that of the pseudo-first-order model. Moreover, the theoretical $q_{e,cal}$ values for both Sb(III) and Cd(II), calculated from the pseudo-second-order model, are closer to the experimental values ($q_{e,exp}$). Therefore, the adsorption behavior of Sb(III) and Cd(II) in binary solution is well described using pseudo-second-order kinetics, which suggests that the adsorption mechanism involves chemisorption.[25]

3.4 Bi-solute (Sb + Cd) adsorption isotherms

The results of experiments employing various initial concentrations of Sb(III) and Cd(II) ions at the optimized pH of 7 with a contact time of 24 h are shown in Fig. 2e and f, respectively. The adsorption capacities for both Sb(III) and Cd(II) increased

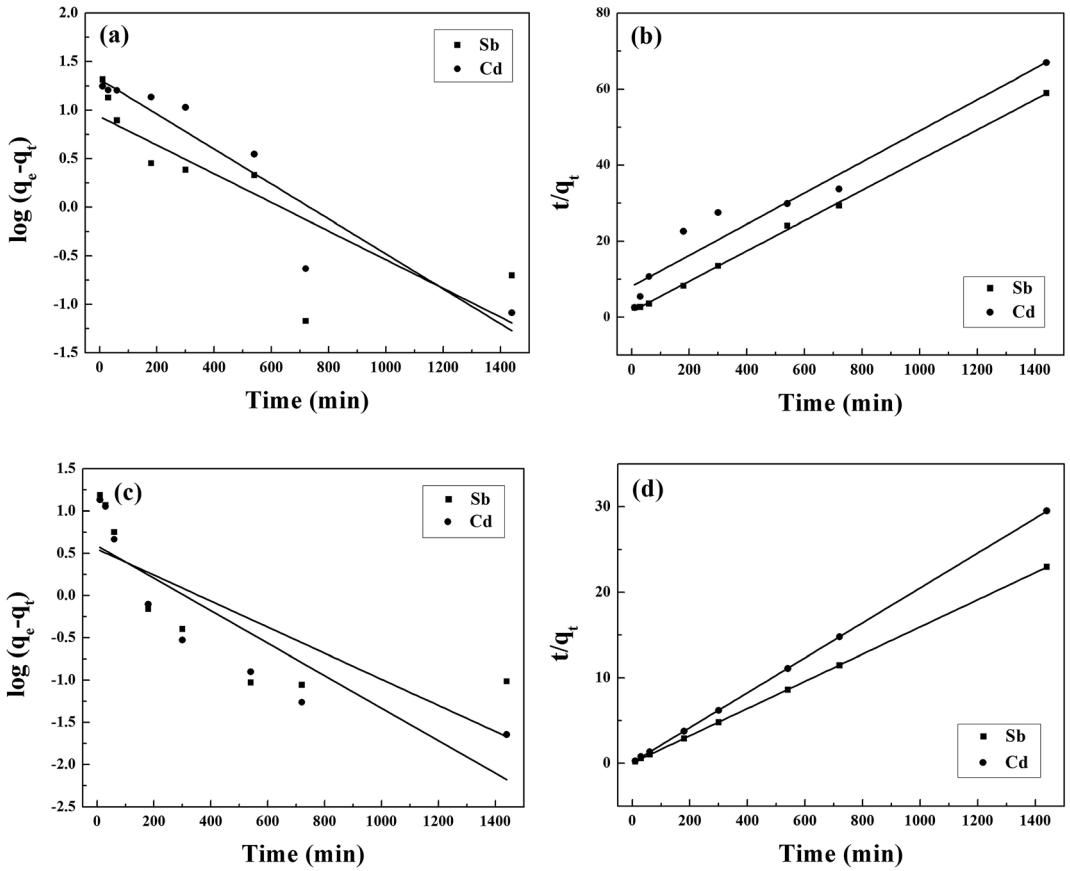

Fig. 3 (a and c) Pseudo-first order and (b and d) pseudo-second order kinetics sorption data for the adsorption of Sb(III) and Cd(II) in a binary system using BC (a and b) and $MnFe_2O_4$–BC (c and d).

significantly with an increase in the initial concentration of Sb(III) and Cd(II) from 100 to 500 mg L^{-1}. The experimental data were fitted with Langmuir and Freundlich isotherm models.[26,27] The linear forms of the Langmuir and Freundlich isotherms are given by eqn (5) and (6), respectively:

$$\frac{C_e}{q_e} = \frac{1}{q_{max}K_L} + \frac{C_e}{q_{max}} \quad (5)$$

$$\ln q_e = \ln K_F + \frac{1}{n}\ln C_e \quad (6)$$

where C_e (mg L^{-1}) is the equilibrium concentration of Sb(III) or Cd(II), and q_e (mg g^{-1}) represents the amount of adsorbed Sb(III) or Cd(II) per unit mass of biochar. q_{max} (mg g^{-1}) indicates the adsorption capacity, whereas K_L (L mg^{-1}) is the Langmuir affinity constant. For the Freundlich isotherm, K_F signifies the adsorption affinity, while n is an indicator related to the heterogeneity of the adsorbent surface.

The fits to the Langmuir and Freundlich models are shown in Fig. 4, and the isotherm parameters are listed in Table 2. For the adsorption of Sb(III) using BC, the Freundlich model provides a better fit for the experimental data than the Langmuir model (Fig. 5a), whereas the adsorption isotherms from Cd(II) are better fitted using the Langmuir model (Fig. 5b). This suggests that Sb(III) adsorption on pristine biochar is a multilayer adsorption process, whereas Cd(II) follows a monolayer

Table 1 Pseudo-first-order and pseudo-second-order kinetic parameters for Sb(III) and Cd(II) adsorbed using BC and $MnFe_2O_4$–BC in a binary system

		Experimental parameters		Pseudo-first order			Pseudo-second order		
Sample	Ion	pH	$q_{e,exp}$ (mg g^{-1})	k_1 (min^{-1})	$q_{e,cal}$ (mg g^{-1})	R^2	k_2 (g mg^{-1} min^{-1})	$q_{e,cal}$ (mg g^{-1})	R^2
BC	Sb(III)	7	24.60	0.0034	8.59	0.636	0.0010	25.11	0.999
BC	Cd(II)	7	21.60	0.0041	20.85	0.885	2×10^{-6}	21.52	0.934
$MnFe_2O_4$–BC	Sb(III)	7	62.80	0.0035	3.55	0.551	0.0040	62.93	0.999
$MnFe_2O_4$–BC	Cd(II)	7	48.80	0.0044	3.89	0.743	0.024	48.99	0.999

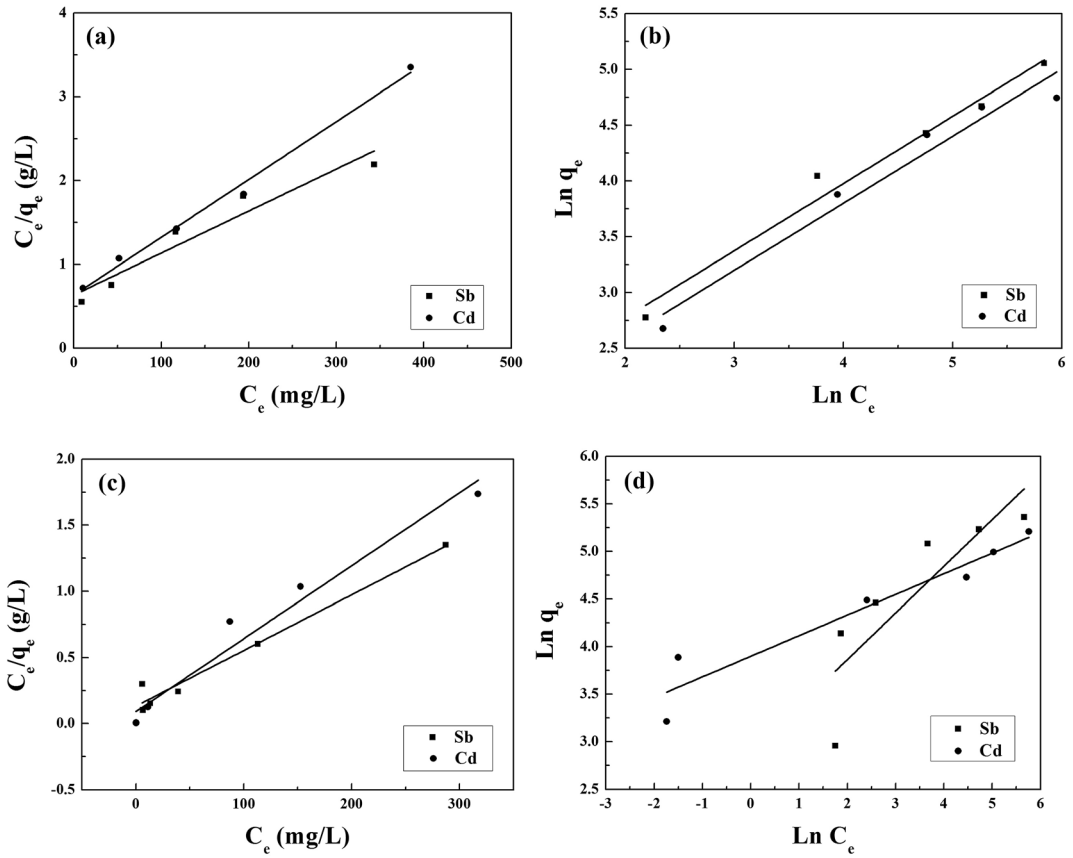

Fig. 4 (a and c) Langmuir and (b and d) Freundlich isotherms for the adsorption of Sb(III) and Cd(II) onto BC (a and b) and $MnFe_2O_4$–BC (c and d) in a binary system.

adsorption process. Moreover, the maximum adsorption capacities calculated from the Langmuir model for BC in the bi-solute system are 199.60 and 145.13 mg g^{-1} for Sb(III) and Cd(II) ions, respectively. Nevertheless, a different scenario is observed for $MnFe_2O_4$–BC. As shown in Fig. 4c and d and Table 2, the Langmuir isotherms correlate better than the Freundlich ones with the experimental data for both Sb(III) and Cd(II). This implies that Sb(III) and Cd(II) likely form monolayers on $MnFe_2O_4$–BC. In addition, the calculated maximum adsorption capacity, q_{max}, values from the Langmuir model are 237.53 mg g^{-1} for Sb(III) and 181.49 mg g^{-1} for Cd(II), which are higher than the values obtained for BC. The maximum adsorption capacities for Sb(III) and Cd(II) are compared with those reported in the literature (Table 3). The adsorption capacity of $MnFe_2O_4$–BC is also higher than that of pyrochar derived from swine manure,[28] a mercapto-functionalized hybrid sorbent,[29] hematite modified magnetic nanoparticles,[30] graphene,[31] biochar derived from *Sida Hermaphrodita*,[32] titanate nanotubes,[33] chitosan crosslinked with epichlorohydrin–triphosphate,[34] and manganese dioxide.[35] Therefore, the $MnFe_2O_4$–BC composite prepared in this study is a possible efficient adsorbent for the removal of Sb(III) and Cd(II).

For comparison, the influence of ionic concentration on the removal of either Sb(III) or Cd(II) was investigated for single solute solutions. However, only 11.4% of Sb(III) was absorbed by BC when the initial Sb(III) concentration was 25 mg L^{-1}. This is because the surface of pristine biochar (BC) has a predominantly net negative charge (as shown in Fig. 1b), and therefore the removal of Sb(III) was limited. The Sb(III) adsorption isotherms for BC are not shown. The effect of the initial Sb(III) or

Table 2 Langmuir and Freundlich parameters for Sb(III) and Cd(II) adsorbed using BC and $MnFe_2O_4$–BC in a binary system

		Langmuir constants			Freundlich constants		
Sample	Ion	K_L (L mg^{-1})	q_{max} (mg g^{-1})	R^2	K_F (mg g^{-1}) (L $mg^{-1})^{1/n}$	n	R^2
BC	Sb(III)	0.00789	199.60	0.912	4.803	1.66	0.973
BC	Cd(II)	0.0109	145.13	0.990	4.038	1.66	0.947
$MnFe_2O_4$–BC	Sb(III)	0.0316	237.53	0.969	17.89	2.04	0.673
$MnFe_2O_4$–BC	Cd(II)	0.00605	181.49	0.960	49.34	4.62	0.900

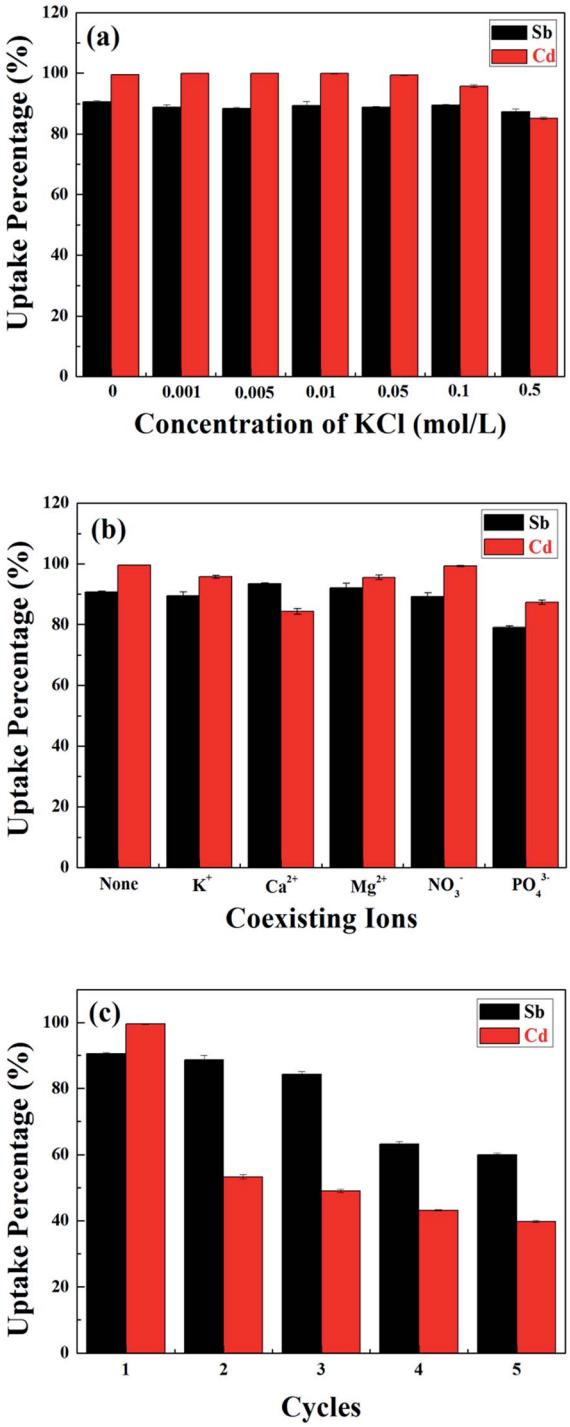

Fig. 5 (a) The effects of KCl concentration on the adsorption of Sb(III) and Cd(II) in binary system removal using $MnFe_2O_4$–BC; (b) the effect of competing ions on Sb(III) and Cd(II) adsorption onto $MnFe_2O_4$–BC in a binary system; and (c) the uptake percentages of Sb(III) and Cd(II) in a mixed solution using $MnFe_2O_4$–BC over five consecutive adsorption–desorption cycles.

Cd(II) concentration on Sb(III) or Cd(II) removal was investigated over the range of 25–500 mg L^{-1}. As shown in Fig. S1a and b,† the adsorption efficiency q_e increased with the initial ionic concentration for both BC and $MnFe_2O_4$–BC, with the latter displaying relatively higher adsorption capacity for each ion. The corresponding adsorption isotherms and isotherm parameters for BC and $MnFe_2O_4$–BC are shown in Fig. S2 and Table S1,† respectively. For both BC and $MnFe_2O_4$–BC, the regression coefficients for the Langmuir adsorption isotherms were higher than those for the Freundlich adsorption isotherms. From the Langmuir adsorption isotherms, the calculated value of the adsorption capacity of BC for Cd(II) is 99.40 mg g^{-1}, whereas the adsorption capacities of $MnFe_2O_4$–BC for Sb(III) and Cd(II) are 159.48 and 122.10 mg g^{-1}, respectively. Therefore, the removal of Sb(III) and Cd(II) using both BC and $MnFe_2O_4$–BC obeys the Langmuir adsorption isotherm, indicating a monolayer adsorption process. In addition, the maximum Sb(III) adsorption capacity (q_{max}) of the system in the absence of Cd(II) is lower than that observed in the presence of Cd(II), for both BC and $MnFe_2O_4$–BC. This result indicates that Cd(II) promotes the removal of Sb(III) using both BC and $MnFe_2O_4$–BC. Meanwhile, the presence of Sb(III) also promotes the removal of Cd(II). Therefore, $MnFe_2O_4$–BC is highly promising for the simultaneous removal of Sb(III) and Cd(II), especially in a bi-solute system.

3.5 Effects of ionic strength

The influence of ionic strength on the removal of Sb(III) and Cd(II) using $MnFe_2O_4$–BC was evaluated, and the results are shown in Fig. 5a. KCl was selected to adjust the ionic strength of the solution to 0, 0.001, 0.005, 0.01, 0.05, 0.1, and 0.5 mol L^{-1}. Apparently, the ionic strength did not have an obvious effect on the removal of Sb(III) and Cd(II) using $MnFe_2O_4$–BC. Only when the KCl concentration reached 0.5 mol L^{-1} did the removal of Sb(III) and Cd(II) using $MnFe_2O_4$–BC slightly decrease. This is because K^+ and Cl^- create steric hindrance for Sb(III) and Cd(II), and act as competitors for the surface adsorption sites on $MnFe_2O_4$–BC, leading to a reduction in the adsorption capacity. Therefore, the above results indicate that the fabricated $MnFe_2O_4$–BC could effectively remove Sb(III) and Cd(II) from water even at ionic strengths of 100 mM.

3.6 Effects of competing ions

Five common ions (K^+, Ca^{2+}, Mg^{2+}, NO_3^-, and PO_4^{3-}) were chosen to investigate the effects of competing ions on Sb(III) and Cd(II) adsorption using $MnFe_2O_4$–BC. As shown in Fig. 5b, none of these five ions have a remarkable effect on the uptake of Sb(III) and Cd(II) under the experimental conditions. Specifically, the presence of K^+, Mg^{2+}, and NO_3^- did not have any noticeable influence on the removal of Sb(III) and Cd(II). In fact, Ca^{2+} could promote the adsorption of Sb(III), while the uptake of Cd(II) was found to decrease in the presence of Ca^{2+} (Fig. 5b). In addition, PO_4^{3-} slightly reduced the uptake of both Sb(III) and Cd(II) under the experimental conditions. These results confirm that Sb(III) and Cd(II) could be effectively removed using $MnFe_2O_4$–BC, despite the presence of competing ions.

3.7 Reusability studies

Reusability is a desirable trait for an effective absorbent. In our experiments, 0.1 mol L^{-1} HCl was chosen as the desorbent. To

Table 3 A comparison of the adsorption capacities of $MnFe_2O_4$–BC for Sb(III) and Cd(II) with those of other reported adsorbents

Adsorbents	Concentration range (mg L^{-1})	pH	Adsorption capacity (mg g^{-1}) Sb(III)	Cd(II)	Ref.
Pyrochar from swine manure	0.1–100/0.3–150	6	13.09	81.32	28
Mercapto-functionalized hybrid sorbent	100–800	5	108.8	—	29
Hematite modified magnetic nanoparticles	1–20	4.1	36.7	—	30
Graphene	1–10	11	8.506	—	31
Biochar derived from *Sida hermaphrodita*	5–500	6	—	35.71	32
Titanate nanotubes	25–300	57	—	65.97	33
Chitosan crosslinked with epichlorohydrin–triphosphate	100–400	5.6	—	83.75	34
Manganese dioxide	0.05–0.7	—	—	176	35
Metal–organic frameworks (MOFs)	10–250		—	225	37
$MnFe_2O_4$–BC	25–500	7	237.53	181.49	This work

study the reusability of $MnFe_2O_4$–BC, adsorption–desorption cycles were repeated five times with the same $MnFe_2O_4$–BC sample. As shown in Fig. 5c, the removal percentages of both Sb(III) and Cd(II) decreased gradually. For the first three cycles, the removal percentage of Sb(III) changed very little. From the third to the fourth cycle, however, there was a decrease of about 20% in the amount of adsorbed Sb(III). Moreover, the removal of Sb(III) ions still reached 60% after the fifth cycle. However, in the case of Cd(II), the situation was different. From the first to the second cycle, the removal percentage of Cd(II) dropped sharply to 53%, and then it declined gradually from the second to the fifth cycle. In the fifth cycle, the removal percentage of Cd(II) ions was found to be ~40%. Thus, the reusability is not satisfactory with regards to Cd(II). This might be because Sb(III) and Cd(II) in solution compete for the adsorption sites on the surface of the $MnFe_2O_4$–biochar nanocomposite. Further, the adsorption capacity of the $MnFe_2O_4$–biochar nanocomposite for Sb(III) is better than for Cd(II). Therefore, the reusability is not good for Cd(II) compared to Sb(III).

3.8 Adsorption mechanism

The surface states of $MnFe_2O_4$–BC after the adsorption of Sb(III) and Cd(II) were studied using FT-IR and XPS to ascertain the mechanism of Sb(III)/Cd(II) adsorption on $MnFe_2O_4$–BC. FT-IR and full-range XPS spectra of $MnFe_2O_4$–BC after adsorption are shown in Fig. 6a and b, respectively. Compared to the IR spectrum of the original $MnFe_2O_4$–BC sample (Fig. 1b), a less intense band at ~3400 cm^{-1} is observed in the spectrum of $MnFe_2O_4$–BC after the adsorption of Sb(III) and Cd(II). This may be attributed to the deprotonation of hydroxyl groups associated with Fe on the $MnFe_2O_4$–BC surface upon the adsorption of Sb(III) and Cd(II). The vibration peaks at 1604 cm^{-1} and 1454 cm^{-1}, which are ascribed to the vibrations of C=C/C=O and $-CH_2-$, shifted to 1590 cm^{-1} and 1430 cm^{-1} after Sb(III) and Cd(II) adsorption, suggesting that Sb(III) and Cd(II) may interact with the C=C/C=O and $-CH_2-$ groups in the $MnFe_2O_4$–BC samples. Moreover, the chemical composition of $MnFe_2O_4$–BC after Sb(III) and Cd(II) co-adsorption was studied by XPS. Peaks corresponding to O 1s, Cd 3d, N 1s and Sb 3d are clearly identified in the survey scan spectrum (Fig. 6b). The presence of Sb(III) and Cd(II) in the resultant product further verifies the co-adsorption of Sb(III) and Cd(II) onto $MnFe_2O_4$–BC. In addition, the binding energies (BE) of Sb 3d3/2 in Sb_2O_3, Sb_2O_4, and Sb_2O_5 have been reported to be 539.6, 539.8, and 540.2 eV, respectively.[4,36] Our XPS spectra of Sb(III)-adsorbed $MnFe_2O_4$–BC showed an indicative Sb(III) binding energy for Sb 3d3/2 at 540.2 eV, indicating the presence of Sb(V) on the $MnFe_2O_4$–BC surface after adsorption. This indeed demonstrates that Sb(III) is chemically adsorbed on the $MnFe_2O_4$–BC surface. The

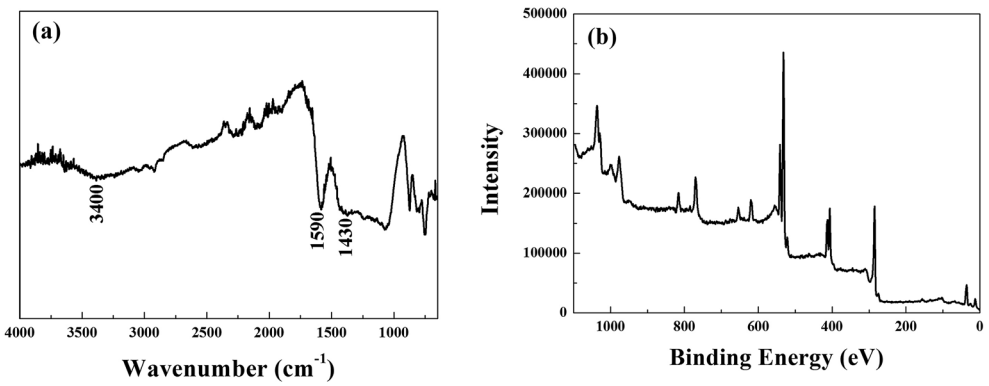

Fig. 6 (a) FT-IR spectrum and (b) XPS spectrum of $MnFe_2O_4$–BC after Sb(III) and Cd(II) co-adsorption.

oxidation mechanism may very well explain the higher Sb(III) adsorption on $MnFe_2O_4$–BC than on pristine BC.

4. Conclusions

In this study, a jacobsite–biochar nanocomposite ($MnFe_2O_4$–BC) was successfully fabricated and its adsorption performance for the removal of Sb(III) and Cd(II) was evaluated. The $MnFe_2O_4$–BC samples exhibited excellent adsorption capabilities and could simultaneously remove Sb(III) and Cd(II) from water. The ionic strength of the solution and coexisting ions did not have an obvious influence on the removal of Sb(III) and Cd(II) using $MnFe_2O_4$–BC, under the examined conditions. Moreover, $MnFe_2O_4$–BC could be used repeatedly. Therefore, the $MnFe_2O_4$–BC fabricated in our study is a promising adsorbent for the simultaneous removal of Sb(III) and Cd(II) from water.

Conflicts of interest

There are no conflicts to declare.

Acknowledgements

This work was supported by the Natural Science Foundation of Zhejiang (LQ17D020002, LY16D010004), the Key Research and Development Projects in Zhejiang Province (2015C03020), and the Zhejiang Provincial Collaborative Innovation Center of Agricultural Biological Resources Biochemical Manufacturing/Zhejiang Provincial Key Lab for Chem & Bio Processing Technology of Farm Products open fund (2016KF0116).

References

1 Z. Wu, M. He, X. Guo and R. Zhou, *Sep. Purif. Technol.*, 2010, **76**, 184–190.
2 S. Guo, P. Jiao, Z. Dan, N. Duan, G. Chen and J. Zhang, *Chem. Eng. J.*, 2017, **317**, 999–1011.
3 M. Krachler, H. Emons and J. Zheng, *Trends Anal. Chem.*, 2001, **20**, 79–90.
4 W. Xu, H. Wang, R. Liu, X. Zhao and J. Qu, *J. Colloid Interface Sci.*, 2011, **363**, 320–326.
5 X. Guo, K. Wang, M. He, Z. Liu, H. Yang and S. Li, *J. Environ. Sci.*, 2014, **26**, 1549–1556.
6 B. Belhalfaoui, A. Aziz, E. H. Elandaloussi, M. S. Ouali and L. C. De Ménorval, *J. Hazard. Mater.*, 2009, **169**, 831–837.
7 D. Sud, G. Mahajan and M. P. Kaur, *Bioresour. Technol.*, 2008, **99**, 6017–6027.
8 M. He, *Environ. Geochem. Health*, 2007, **29**, 209–219.
9 S. Fu and C. Y. Wei, *J. Soils Sediments*, 2013, **13**, 106–116.
10 J. Lehmann, J. Gaunt and M. Rondon, *Mitig. Adapt. Strat. GL.*, 2006, **11**, 395–419.
11 Y. Sun, B. Gao, Y. Yao, J. Fang, M. Zhang, Y. Zhou, H. Chen and L. Yang, *Chem. Eng. J.*, 2014, **240**, 574–578.
12 A. Mukherjee, A. R. Zimmerman and W. Harris, *Geoderma*, 2011, **163**, 247–255.
13 Y. Yao, B. Gao, M. Zhang, M. Inyang and A. R. Zimmerman, *Chemosphere*, 2012, **89**, 1467–1471.
14 Y. Bai, W. A. Jefferson, J. Liang, T. Yang and J. Qu, *J. Environ. Sci.*, 2017, **54**, 126–134.
15 P. Qi and T. Pichler, *Chemosphere*, 2016, **145**, 55–60.
16 Y. Y. Wang, H. H. Lu, Y. X. Liu and S. M. Yang, *RSC Adv.*, 2016, **6**, 83534–83546.
17 X. Xiao, B. L. Chen and L. Z. Zhu, *Environ. Sci. Technol.*, 2014, **48**, 3411–3419.
18 R. Azargohar, S. Nanda, J. A. Kozinski, A. K. Dalai and R. Sutarto, *Fuel*, 2014, **125**, 90–100.
19 Y. Y. Wang, H. H. Lu, Y. X. Liu and S. M. Yang, *Colloids Surf., A*, 2016, **509**, 550–563.
20 Z. Droussi, V. D'orazio, M. R. Provenzano, M. Hafidi and A. Ouatmane, *J. Hazard. Mater.*, 2009, **164**, 1281–1285.
21 B. Chen, Z. Chen and S. Lv, *Bioresour. Technol.*, 2011, **102**, 716–723.
22 A. Han, J. Liao, M. Ye, Y. Li and X. Peng, *Chin. J. Chem. Eng.*, 2011, **19**, 1047–1051.
23 V. M. Bujoreanu, E. Segal, M. Brezeanu, R. Salmon, J. J. Videau and C. Gheorghies, *Thermochim. Acta*, 1996, **288**, 221–237.
24 Y. S. Ho and G. McKay, *Water Res.*, 2000, **34**, 735–742.
25 H. Liu, C. Wang, J. Liu, B. Wang and H. Sun, *J. Environ. Manage.*, 2013, **128**, 727–734.
26 I. Langmuir, *J. Am. Chem. Soc.*, 1918, **40**, 1361–1403.
27 H. M. F. Freundlich, *Z. Phys. Chem.*, 1906, **57**, 385–470.
28 L. Han, H. Sun, K. S. Ro, K. Sun, J. A. Libra and B. Xing, *Bioresour. Technol.*, 2017, **234**, 77–85.
29 H. T. Fan, W. Sun, B. Jiang, Q. J. Wang, D. W. Li, C. C. Huang, K. J. Wang, Z. G. Zhang and W. X. Li, *Chem. Eng. J.*, 2016, **286**, 128–138.
30 C. Shan, Z. Ma and M. Tong, *J. Hazard. Mater.*, 2014, **268**, 229–236.
31 Y. Q. Leng, W. L. Guo, S. N. Su, C. L. Yi and L. T. Xing, *Chem. Eng. J.*, 2012, **211**, 406–411.
32 A. Bogusz, P. Oleszczuk and R. Dobrowolski, *Bioresour. Technol.*, 2015, **196**, 540–549.
33 T. Wang, W. Liu, L. Xiong, N. Xu and J. Ni, *Chem. Eng. J.*, 2013, **215**, 366–374.
34 R. Laus and V. T. de Fávere, *Bioresour. Technol.*, 2011, **102**, 8769–8776.
35 Q. D. Qin, Q. Q. Wang, D. F. Fu and J. Ma, *Chem. Eng. J.*, 2011, **172**, 68–74.
36 R. Delobel, H. Baussart, J. M. Leroy, J. Grimblot and L. Gengembre, *J. Chem. Soc., Faraday Trans. 1*, 1983, **79**, 879–891.
37 H. Xue, Q. H. Chen, F. L. Jiang, D. Q. Yuan, G. X. Lv, L. F. Liang, L. Y. Lia and M. C. Hong, *Chem. Sci.*, 2016, **7**, 5983–5988.